ACS OMEGA

http://pubs.acs.org/journal/acsodf

Article

Experimental Investigation of a Self-adaptive Thickening Polymer Performance under High-Temperature–High-Salinity Reservoir Conditions

Chuangchuang Qi, Mohamed Haroun, Md Motiur Rahman,* Abhijith Suboyin, Jassim Abubacker Ponnambathayil, and Bisweswar Ghosh

Cite This: *ACS Omega* 2023, 8, 24426–24440

Read Online

ACCESS | Metrics & More | Article Recommendations

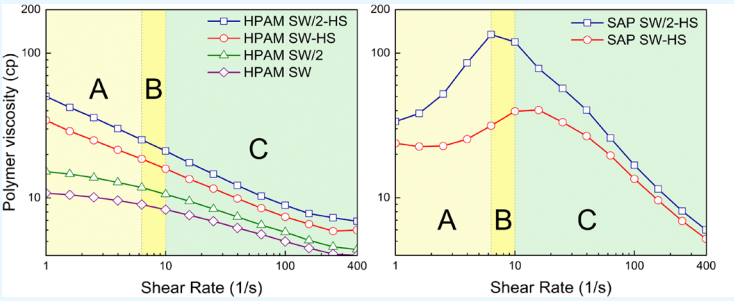

Region	Shear-Thickening	Shear-Thinning
A	SAP SW/2-HS	All HPAM
A+B	SAP SW-HS	All HPAM
C	N/A	All HPAM and SAP

ABSTRACT: A polymer flooding workflow was developed to diminish polymer degradation and minimize formation damage under high-temperature–high-salinity reservoir conditions by using a shear-thickening polymer (SAP) prepared in engineered waters. First, rock characterization, fluid–fluid analysis, and formation damage tests were conducted to shortlist the potential formulations of polymer solutions based on higher viscosity and less formation damage. Second, polymer core flooding experiments were conducted under reservoir conditions to investigate the performance of candidate polymer solutions on oil displacement efficiency (DE). For the first time, the compatibility between SAP and engineered water was systematically tested. The factors affecting bulk rheology, polymer retention, and oil DE, including polymer concentration, polymer type, salinity, and hardness, were experimentally investigated and compared with regular partially hydrolyzed polyacrylamide (HPAM). Results showed that compared with HPAM, the SAP solution led to lower formation damage and overall higher oil DE, especially in the first 0.4 pore volume of polymer injection. When using SAP prepared in twice-diluted and hardness-stripped seawater under low-salinity formation brine conditions, the DE was the highest (69.04%). The formation damage was reduced when the salinity and hardness of the base fluid were lower, whereas stripping the hardness had a more pronounced effect on reducing formation damage. The improved oil recovery potential due to the shear-thickening feature of SAP solutions and their better compatibility with engineered water compared to regular HPAM has been proven in this study. It was also found that the lower salinity and hardness of the engineered water further stimulated the enhanced oil recovery potential of SAP solutions. The contribution of this work relies on revealing how SAP prepared in different engineered waters affects incremental oil DE under harsh reservoir conditions based on experimental evidence and mechanism analysis. The novelty of this work lays the foundation for investigating the potential application of SAP on a pilot scale.

1. INTRODUCTION

Globally, oil and gas consumption has been increasing, while more than 65% of the original oil in place remains in the reservoirs after conventional primary recovery and secondary recovery.[1] This portion of oil might either be bypassed by injected fluid owing to reservoir heterogeneity and viscosity contrast (gravity contrast) or be trapped by capillary forces in the flooded area. Enhanced oil recovery (EOR) methods have been applied to recover oil in mature fields by increasing the volumetric sweep efficiency and/or displacement efficiency.[2] Polymer flooding is a chemical EOR technique widely used in fields to recover bypassed oil. The injection of polymer solutions might increase the viscosity of the displacing fluid, thus lowering the water–oil (displacing fluid to displaced fluid) mobility ratio, leading to a higher volumetric sweep efficiency.[3] Reduction of viscous fingering and improvement of the water injection profile after polymer flooding contribute to

Received: March 24, 2023
Accepted: June 1, 2023
Published: June 27, 2023

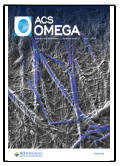

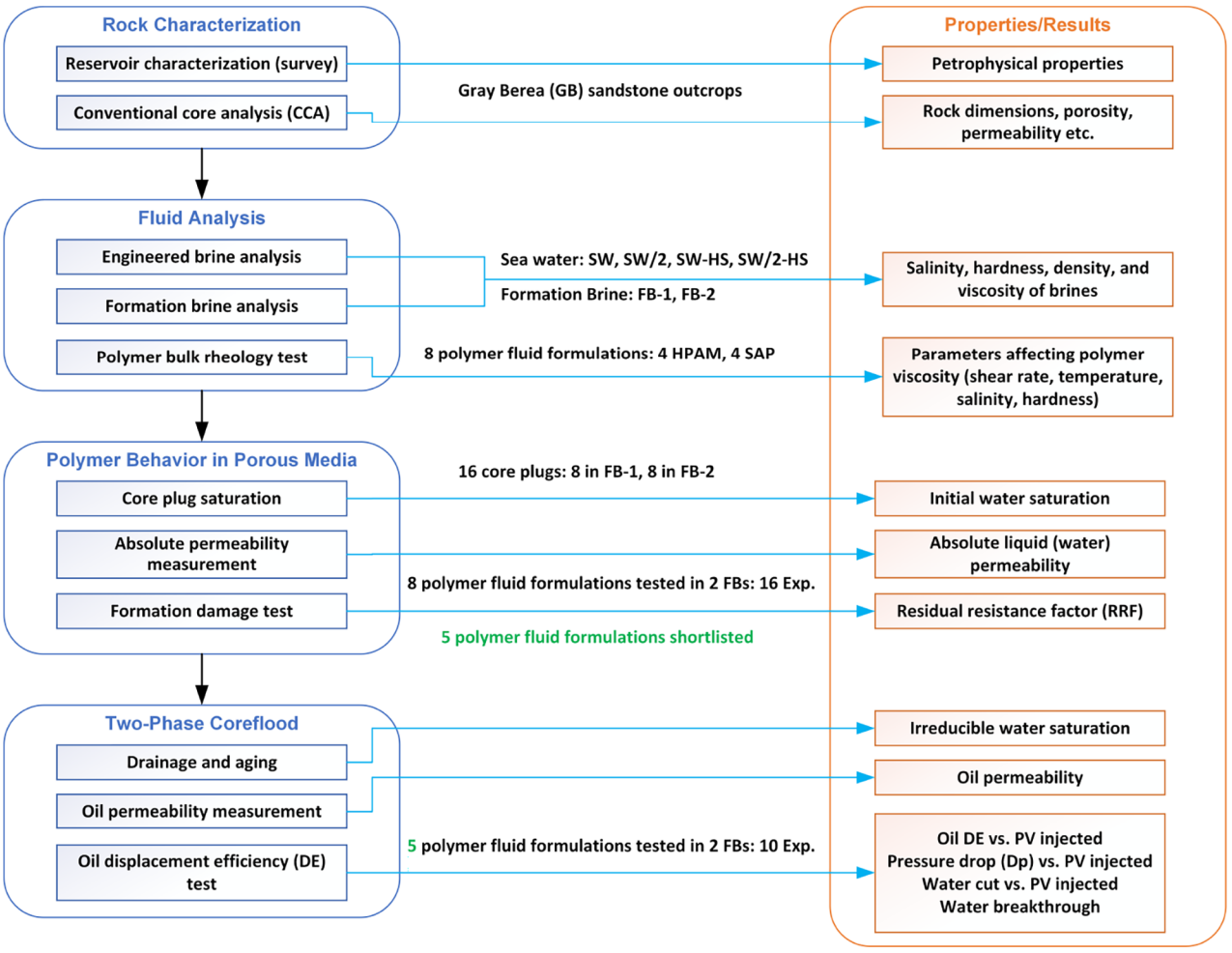

Figure 1. Flow chart of the work procedure.

minimizing the bypassing effect.[4] Polymer flooding has been conducted in many fields for decades and has successfully increased oil recovery.

Nevertheless, fluid incompatibility under harsh reservoir conditions and poor conformance in heterogeneous reservoirs hinder the performance of polymer flooding.[5,6] Harsh reservoir conditions hinder the polymer EOR performance because of the incompatibility between the reservoir fluid and the injected polymer solution, leading to unexpected formation damage and unfavorable EOR efficiency. Many factors affecting polymer core-flood performance have been reported in laboratory investigations, such as temperature, formation brine condition, polymer type, polymer concentration with smart brine, and injection scheme.[6−11] Smart water flooding has been investigated to alter the rock wettability of high-temperature carbonate reservoirs by spiking phosphate.[12] In this study, new associative polymers prepared in different formulations of engineered water have been tested to improve polymer flooding performance under harsh reservoir conditions.

Associative polymers are copolymers of a hydrophilic acrylamide monomer with a small amount of a hydrophobic monomer (0.3−4 mol %), leading to some advantages of associative polymers, such as greater viscosities than HPAM with similar molecular weight, relative insensitivity to salinity or temperature, and less overall polymer use in large-scale polymer flooding.[13] Rheological properties, polymer transport, and oil recovery efficiency have been investigated.[13] The shear-thinning feature of HPAM is beneficial for the polymer injection process because the low viscosity of the polymer solution might enhance the polymer injectivity near the wellbore, while in reservoirs, this feature is a drawback because the flow velocity in the high-permeability zone would be high, leading to lower polymer viscosity.[13] The shear-thickening feature is favorable in communicated multilayered reservoirs because it is more effective in displacing bypassed oil in the low-permeability zone. Thus, the ideal characteristic of a polymer solution is that its viscosity is lower in the near-wellbore region and higher in the high-permeability layers of a communicated multilayered reservoir. At the real field scale, the typical field water injection rate is approximately 1 ft/day. In this shear-rate region of field polymer implementation, the HPAM usually only exhibits shear-thinning features.[14]

Researchers have developed or tested polymers that exhibit shear-thickening features at moderate flow velocities and shear-thinning features at high flow velocities. These polymers are known as bifunctional or associative polymers.[14−17] Nevertheless, it is difficult to control their viscosity change versus the flow rate in the reservoir. Adjusting these polymer solutions to fit the different flow velocities and salinity requirements of different reservoirs remains an issue. Few studies have been conducted on the EOR performance of shear-thickening polymers. This study investigated how the ion composition of a base fluid (engineered water) interacts with polymer molecules and thus affects the rheology, formation damage,

https://doi.org/10.1021/acsomega.3c01984
ACS Omega 2023, 8, 24426−24440

and displacement efficiency of polymer fluids under harsh reservoir conditions. The performance of conventional HPAM and shear-thickening polymer SAP prepared with different formulations of engineered brine was studied under two different formation brine conditions.

This research focuses on understanding the factors affecting the behavior of conventional HPAM and associative polymer SAP and improving their EOR performance under harsh reservoir conditions (high temperature and high salinity) by conducting rock characterization, fluid analysis, and core-flood experiments. The key objectives are to experimentally investigate the factors affecting the bulk rheology, polymer retention, and oil displacement efficiency of SAP and compare it with regular HPAM under harsh reservoir conditions. This study contributes to revealing the compatibility between shear-thickening associative polymers and different engineered water formulations and their performance in incremental oil displacement efficiency under harsh reservoir conditions based on experimental evidence and mechanism analysis.

The degradation and conformance control problems during polymer flooding and the characteristics of shear-thickening polymers are introduced in Section 1. The remainder of this paper is organized as follows. In Section 2, the materials and methodology used in this study for the comprehensive investigation of polymer performance are provided. Section 3 focuses on the results of the fluid analysis and core-flood experiments. These results reveal how multiple parameters affect the EOR performance of HPAM and SAP under harsh reservoir conditions, including the salinity and hardness of the engineered brine, composition of the formation brine, and temperature. In Section 4, the main conclusions based on the experimental results and discussion are presented.

2. MATERIALS AND METHODS

A polymer flooding workflow was developed to investigate the performance of a shear-thickening polymer SAP compared to that of the conventional polymer HPAM under harsh reservoir conditions. First, information regarding the geological background of the targeted reservoir field was acquired, and a conventional core analysis was conducted. Fluid analysis and formation damage tests were then conducted to understand the bulk rheology of the polymer solutions and their behavior in porous media. Five out of the eight polymer fluid formulations were shortlisted after the formation damage test. Finally, oil displacement efficiency experiments were conducted under reservoir conditions to investigate the effect of the candidate polymer solution on the oil displacement efficiency. A flowchart of the work procedure is shown in Figure 1.

2.1. Materials. *2.1.1. Sandstone Rock.* Gray Berea sandstone outcrops had a length of 1 ft and a diameter of 1.5 in. Each outcrop was cut and trimmed to four core samples with a length of approximately 3 in. In this study, 26 cores were used for the core-flooding experiments, including 16 cores for the formation damage test and 10 cores for the oil displacement efficiency study. The cores were regarded as homogeneous, with the average porosity ranging from approximately 18 to 21% and the absolute permeability ranging from approximately 100 to 130 md.

The geological background and reservoir characterization of the targeted field have been well summarized by Qi et al.[18] and Rabbani et al.[19] Based on field data, representative core plugs cut from Gray Berea sandstone outcrops were chosen for the polymer core-flood experiments. Sixteen core plugs (batch 1) were used for the formation damage test, and 10 core plugs (batch 2) were used for the polymer core-flood oil displacement efficiency study. A summary of their properties is presented in Table 6 and Table 7.

2.1.2. Synthetic Brine. The formation brine was synthetically prepared by dissolving the salts in deionized water. Two formulations of the formation brine were prepared according to the reservoir fluid composition: FB-1 (28,230 ppm, 2.823 wt %) and FB-2 (79,708 ppm, 7.9708 wt %). The composition of the synthetic formation brine is illustrated in Table 1, and the properties of the formation brine under reservoir temperature (80 °C) are illustrated in Table 2.

Table 1. Composition of Formation Brine

composition (mg/L)	formation brine 1 (FB-1)	formation brine 2 (FB-2)
Na^+	9960	27,708
Ca^{2+}	581	2265
Mg^{2+}	225	656
Cl^-	16,382	47,516
$SO4^{2-}$	762	1405
$HCO3^-$	317	146

Table 2. Properties of Formation Brine under the Reservoir Temperature (80 °C)

fluid	density (g/cm^3)	viscosity (cP)
FB-1	0.97	0.39
FB-2	1.02	0.41

2.1.3. Base Fluid and Polymer. Four formulations of seawater were synthetically prepared as base fluids of polymer solutions: normal seawater (SW, 13,464 ppm, 1.3464 wt %), twice-diluted seawater (SW/2, 6732 ppm, 0.6732 wt %), hardness-stripped seawater (SW -HS, 14,241 ppm, 1.4121 wt %), and twice-diluted hardness-stripped seawater (SW/2-HS, 7121 ppm, 0.7121 wt %). The composition of the seawater is shown in Table 3.

Table 3. Composition of Seawater

composition (mg/L)	SW	SW/2	SW-HS	SW/2-HS
Na^+	3336	1668	5230	2615
Ca^{2+}	361	180	0	0
Mg^{2+}	756	378	0	0
Cl^-	5531.00	2766	5531	2766
$SO4^{2-}$	3260	1630	3260	1630
HCO_3^-	220	110	220	110

MAX-165 and SAP-1386 were used in this study (Table 4). MAX-165 is a regular HPAM polymer, and SAP-1386 is an associated polymer with self-adaptive thickening features. In this study, 1000 and 2000 ppm were chosen as concentrations of polymer solutions based on the recommendation of the manufacturer, which is in line with the literature.[6,8,11]

2.1.4. Crude Oil. Light crude oil was used to drain the formation brine in core plugs. Crude oil has a density of 0.7843 g/cm^3 and a viscosity of 1.2318 cP at a reservoir temperature of 80 °C. Table 5 lists the density and viscosity at varying temperatures.

2.1.5. Rock Samples. Based on the field data, representative core plugs cut from Gray Berea sandstone outcrops were

https://doi.org/10.1021/acsomega.3c01984
ACS Omega 2023, 8, 24426−24440

Table 4. Properties of Polymers

name	source	manufacture	type	molecular weight (million Daltons)
MAX-165	ChemEOR, Inc.	ChemEOR, Inc.	HPAM polymer	15
SAP-1386	SGTC[a]	PEERi[b]	associative polymer	0.5

[a]SGTC: Sheeta Global Tech Corp, Covina, CA 91722, U.S.A. [b]PEERi: Power, Environmental & Energy Research (PEER) Institute, Covina, CA 91722, U.S.A.

Table 5. Density and Viscosity of Crude Oil

temperature	density	dynamic viscosity	kinematic viscosity
0 °C	0.8271 g/cm^3	3.8820 cP	4.6938 mm^2/s
40 °C	0.8130 g/cm^3	2.3840 cP	2.9324 mm^2/s
80 °C	0.7843 g/cm^3	1.2318 cP	1.5706 mm^2/s

chosen for the polymer core-flood experiments. Sixteen core plugs (batch 1) were used for the formation damage test, and 10 core plugs (batch 2) were used for the polymer core-flood oil displacement efficiency study. The summary of their properties is shown in Tables 6 and 7.

2.2. Methods. *2.2.1. Polymer Bulk Rheology Tests.* Bulk rheology tests were conducted to investigate the effects of the polymer type, polymer concentration, solution brine salinity, solution brine hardness, temperature, and shear rate on the viscosity of the polymer solutions. The study was conducted using a stress-controlled shear rheometer (Discovery HR-3, DHR-3, TA Instrument) provided by Anton Paar.

The targeted shear rate region was calculated according to the rock properties and injection rates.[20] Equation 1 was applied for calculation. The reference shear rate region for the bulk rheology test ranged from 1 to 400 s^{-1}.

$$\gamma_w = \frac{3n+1}{4n} \times \frac{4q}{A[8k\phi]^{1/2}} \quad (1)$$

where γ_w is the shear rate in s^{-1}, q is the flow rate in cm^3/sec, A is the cross-sectional area in cm^2, k is the absolute permeability in cm^2 (1 cm^2 ≅ 10^{11} md), and the term $(3n + 1)/4n$ represents the non-Newtonian correction factor that can be omitted at very low flow rates.

The viscosity of the polymer solutions was measured at 25 °C under shear rates varying from 1 to 400 s^{-1}. At a fixed shear rate of 10 s^{-1}, the viscosity of the polymer solutions was measured at temperature ranging from 25 to 60 °C to investigate the effect of temperature. Rheology tests above 60 °C were not conducted because they require the application of high pressures. The current temperature range was selected to characterize the thermal degradation of polymers. Eight HPAM and four SAP solutions were tested.

In the oil displacement efficiency study, the shear rate corresponding to the injection rate was estimated using eq 1. For Gray Berea sandstone, the shear rate corresponding to a typical injection rate of 1 ft/day in the core-flooding experiments was estimated as 7−8 s^{-1}.

2.2.2. Formation Damage Test. The residual resistance factor (RRF) reflects the reduction in permeability caused by polymer injection in a porous medium. It is defined as the ratio of brine mobility before polymer flooding to that after polymer flooding, which can be calculated using the pressure drop ratio during brine injection under two different conditions (eq 2). Because polymer retention is an irreversible process, flushing the core with brine after polymer flooding does not fully restore the permeability of the core. Therefore, the RRF value after polymer flooding is typically greater than 1.

$$\mathrm{RRF} = \frac{\lambda_{w,initial}}{\lambda_{w,after\ polymer}} = \frac{\Delta p_{(brine\ after\ polymer)}}{\Delta p_{(brine\ before\ polymer)}} \quad (2)$$

where λ_w is the water phase mobility; $\lambda_{w,\ initial}$ represents the brine mobility before polymer injection, and $\lambda_{w,\ after\ polymer}$ is the brine mobility after polymer injection; Δp represents the pressure drop during injection of brine; $\Delta p_{(brine\ before\ polymer)}$ represents the pressure drop measured during brine injection prior polymer flooding; and $\Delta p_{(brine\ after\ polymer)}$ represents the stabilized pressure drop measured during brine injection after polymer flooding.

The key objective of the formation damage test is to investigate the formation damage effect of shortlisted polymer solutions in porous media under different formation brine conditions by evaluating the RRF. The effects of polymer type,

Table 6. Properties of Core Plugs Used for the Formation Damage Test

no.	core plug ID	length (cm)	diameter(cm)	dry weight (g)	grin density (g/mL)	helium porosity	air permeability (md)
1	GB 2-1	7.54	3.78	178.4	2.65	20.66%	187.9
2	GB 2-2	7.54	3.78	178.2	2.65	20.63%	195.3
3	GB 1-3	7.57	3.76	176.1	2.64	21.02%	225.1
4	GB 2-3	7.39	3.76	173.0	2.64	20.44%	191.3
5	GB 4-3	7.26	3.78	170.6	2.64	21.01%	201.7
6	GB 3-3	7.49	3.78	175.7	2.64	20.39%	208.3
7	GB 1-2	7.44	3.78	174.8	2.65	21.40%	216.3
8	GB 3-1	7.59	3.78	179.3	2.66	20.85%	216.3
9	GB 1-4	7.57	3.81	185.5	2.63	18.37%	159.8
10	GB 3-4	7.21	3.81	177.9	2.65	18.40%	144.8
11	GB 4-4	7.39	3.81	181.8	2.65	18.41%	144.4
12	GB 2-4	7.24	3.81	177.3	2.64	19.76%	160.2
13	GB 1-5	7.50	3.83	182.1	2.65	20.36%	174.4
14	GB 9-5	7.54	3.76	177.8	2.65	19.91%	152.5
15	GB 10-5	7.47	3.76	176.1	2.66	20.15%	156.3
16	GB 12-5	7.50	3.76	176.7	2.64	19.70%	175.4

https://doi.org/10.1021/acsomega.3c01984
ACS Omega 2023, 8, 24426−24440

Table 7. Properties of Core Plugs Used for Oil Displacement Efficiency Study

no.	core plug ID	length (cm)	diameter (cm)	pore volume (cm^3)	helium porosity	air permeability (md)	absolute permeability (md)
1	GB 2-5	7.30	3.83	17.55	20.87%	160.9	96.9
2	GB 3-5	7.25	3.83	16.84	20.16%	172.0	113.9
3	GB 4-5	7.40	3.83	17.49	20.52%	173.6	106.5
4	GB 5-5	7.59	3.83	17.67	20.20%	164.9	109.1
5	GB 6-5	7.42	3.83	17.39	20.34%	163.8	98.4
6	GB 8-5	7.31	3.83	17.41	20.68%	160.6	94.4
7	GB 11-5	7.23	3.76	15.45	19.24%	172.9	112.8
8	GB 13-5	7.59	3.75	17.26	20.59%	184.7	127.1
9	GB 15-5	7.42	3.75	16.92	20.65%	200.0	135.2
10	GB 16-5	7.53	3.75	16.23	19.51%	195.6	113.8

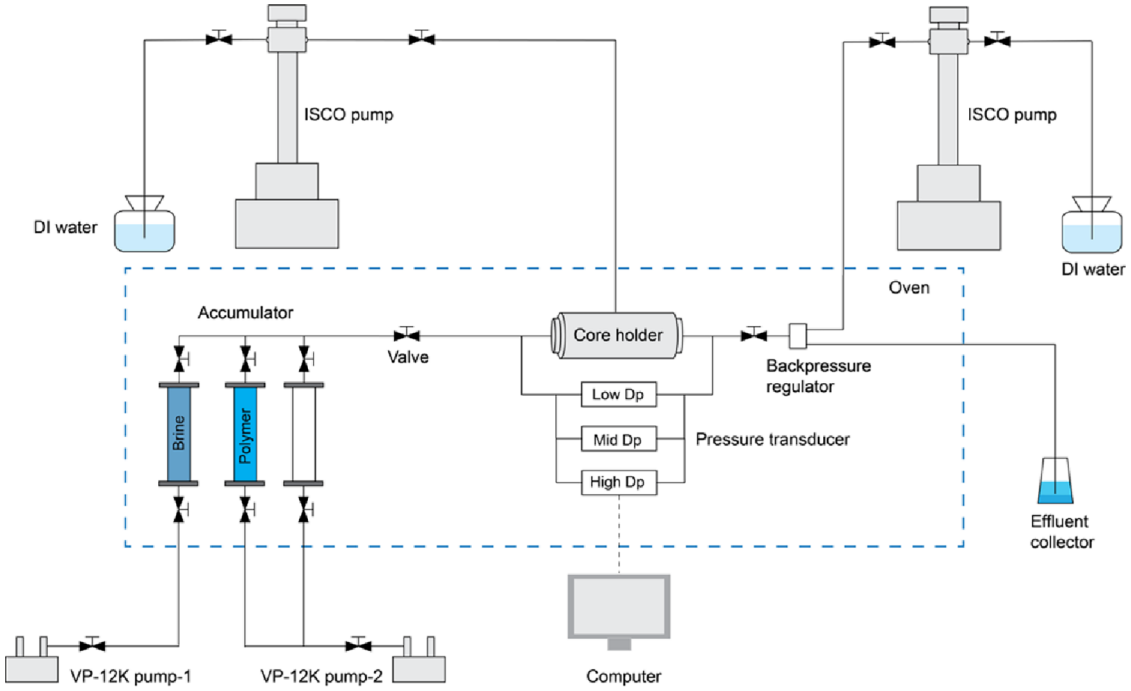

Figure 2. Schematic diagram of the core-flood system of the formation damage test.

Table 8. Details of Core Plugs Used for Oil Displacement Experiments

sample ID	kw (mD)	PV (cm^3)	brine volume (cm^3)	Swir	polymer	formation brine
GB 3-5	113.9	16.84	12.0	28.74%	HPAM SW	FB-1
GB 15-5	135.2	16.92	12.3	27.30%	SAP SW	FB-1
GB 13-5	127.1	17.26	12.8	25.84%	SAP SW-HS	FB-1
GB 5-5	109.1	17.67	12.3	30.39%	SAP SW/2	FB-1
GB 11-5	112.8	15.45	11.5	25.57%	SAP SW/2-HS	FB-1
GB 8-5	94.4	17.41	11.7	32.80%	HPAM SW	FB-2
GB 4-5	106.5	17.49	12	31.39%	SAP SW	FB-2
GB 2-5	96.9	17.55	12.8	27.07%	SAP SW-HS	FB-2
GB 16-5	113.8	16.23	13.1	19.29%	SAP SW/2	FB-2
GB 6-5	98.4	17.39	11.5	33.87%	SAP SW/2-HS	FB-2

salinity, hardness of base fluids, and formation brine type on the formation damage effect were studied. Sixteen formation damage experiments were conducted using eight different polymer solutions under two formation brine conditions (FB-1 and FB-2).

This study was conducted using a core-flood system under the condition of a confining pressure of 3000 psi, backpressure of 1000 psi, and temperature of 80 °C. The flow rates in each experiment were 0.5, 1.0, 2.0, 3.0, and 4.0 cm^3/min. The stabilized pressure drop at each flow rate was recorded, and the RRF was calculated accordingly. A schematic of the experimental setup is shown in Figure 2.

2.2.3. Drainage and Core Aging. Drainage involves injecting oil into core plugs to reach irreducible water saturation. Core holders, water-wet porous plates, hand pumps, oil accumulators, and injection pumps were used for the drainage. The core plugs were fully saturated with formation brine prior to drainage.

https://doi.org/10.1021/acsomega.3c01984
ACS Omega 2023, 8, 24426−24440

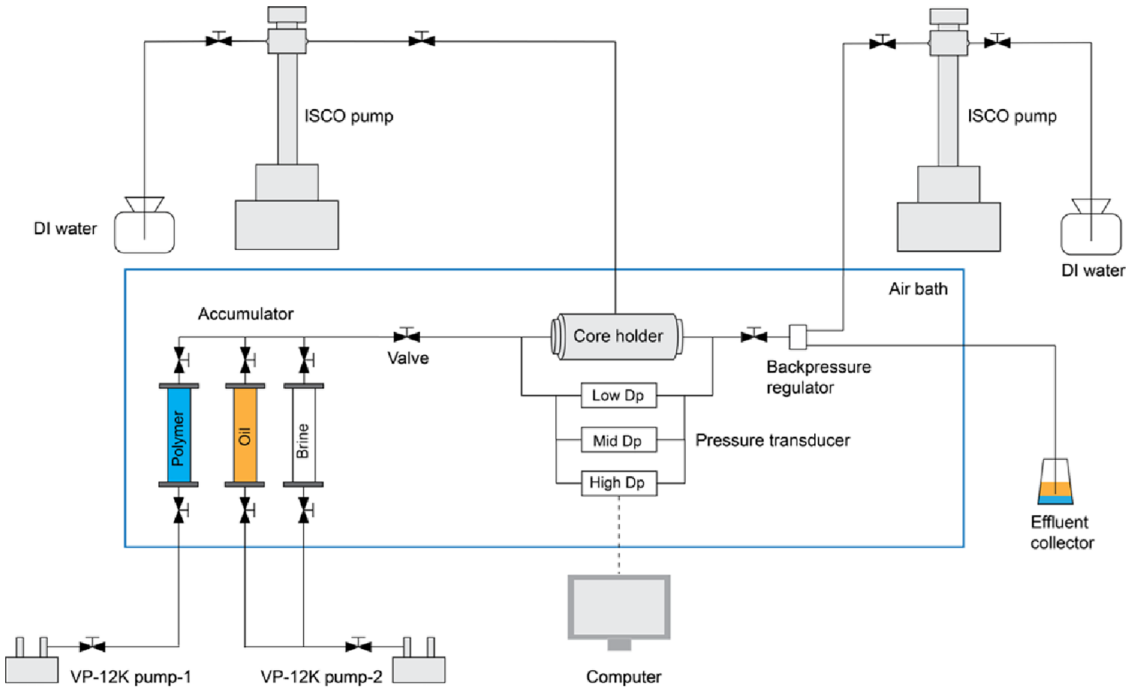

Figure 3. Schematic diagram of the core-flood system.

Each core plug is placed in the sleeve of the core holder. A water-wet porous plate is placed at the bottom of the core plug. This allowed the water phase to pass through and prevented the oil phase from passing. After applying a confining pressure of 1000 psi, the filtered crude oil was injected from the accumulator into the core holders. The injection pressure was initially set to 40 psi and after approximately 72 h, it was increased to 180 psi. The duration of the drainage process for each sample batch was approximately 120 h.

The effluent (brine) was collected using a graduated tube. At the end of the drainage, the volume of the brine produced stabilized. This stabilized volume was used to calculate irreducible water saturation (Swir).

The results are summarized in Table 8, which illustrates the Swir values of each sample used in the oil displacement efficiency experiments. Swir values ranged from 19.29 to 33.87%. The plan and core information for the oil displacement efficiency experiments are presented in Table 8. The absolute permeability of these core plugs ranged from approximately 90 to 140 md. Half of them were saturated with FB-1, and half were saturated with FB-2.

The effective permeability to oil of each core plug was measured using a core-flood system under a confining pressure of 1000 psi, backpressure of 200 psi, and temperature of 80 °C. The temperature was increased to 80 °C because it was difficult for the pressure drop to stabilize at ambient temperature when using crude oil.

Different flow rates were used for each measurement, which were 0.5, 1.0, 1.5, and 2.0 cm^3/min, respectively. The oil permeability was calculated using Darcy's equation (eq 3):

$$q = \frac{k_o}{\mu_o} A \frac{\Delta P}{L} \tag{3}$$

where q is the flow rate in cm^3/s, k_o is the oil permeability in Darcy, μ represents the dynamic viscosity of crude oil in cP, ΔP is the pressure drop in atm, L is the length of the core plug in cm, and A is the cross-sectional area of the core plug in cm^2.

After the oil permeability measurement, the samples were placed into the aging cells and crude oil was added to keep the samples submerged below the oil level. The well-sealed aging cells were placed in an oven at 90 °C for 7 days to restore the wettability of the reservoir.

After aging, the oil permeabilities of these core plugs were measured using a core-flood system under a confining pressure of 1000 psi, backpressure of 200 psi, and temperature of 80 °C to determine the permeability change after aging. Subsequently, the confining pressure was increased to 3000 psi, and the backpressure was increased to 1000 psi. The oil permeability of each core plug was measured again under this condition (reservoir condition). This was to guarantee that the oil permeability was measured under the same reservoir conditions as in the formation damage test and oil displacement efficiency experiment. The flow rates used in each measurement were 0.5, 1.0, 1.5, and 2.0 cm^3/min.

2.2.4. Oil Displacement Efficiency Study. An oil displacement efficiency study was conducted using a core-flood system under reservoir conditions (2000 psi confining pressure, 1000 psi backpressure, and 80 °C), as illustrated in Figure 3. First, filtered crude oil was injected through the core sample for permeability measurements. Subsequently, the polymer solution was injected from another accumulator to displace oil. After polymer injection of one dead volume, the effluent was collected in graduation tubes by using a fraction collector. The fraction collector automatically switches the 5 cm^3 graduated tubes every specified duration.

The flow rates were 0.05 cm^3/min (1 ft/day), 0.1 cm^3/min (2 ft/day), 0.5 cm^3/min (10 ft/day), and 1.0 cm^3/min (20 ft/day), respectively. In each experiment, 1.6 PV of the polymer solution was injected at a flow rate of 0.05 cm^3/min. At each flow rate except at 0.05 cm^3/min, approximately 2 PV of polymer solution was injected. The duration of each oil displacement efficiency experiment was approximately 30 h.

https://doi.org/10.1021/acsomega.3c01984
ACS Omega 2023, 8, 24426−24440

The oil production data (oil displacement efficiency), water cut, and pressure drop were analyzed, as shown in eqs 4 and 5.

$$\mathrm{DE} = \frac{V_{ot}}{(1 - S_{wir}) \times V_p} \tag{4}$$

where DE represents the oil displacement efficiency, V_{ot} represents the cumulative oil production in cm^3, S_{wir} is the irreducible water saturation, and V_p represents the pore volume of the core plug in cm^3.

$$W_c = \frac{V_w}{V_o + V_w} \tag{5}$$

where W_c represents the water cut, V_o represents the oil production in a specific duration in cm^3, and V_w represents the water production for a specific duration in cm^3.

3. RESULTS AND DISCUSSION

3.1. Polymer Bulk Rheology. The concentration effect on the viscosity of HPAM under 25 and 60 °C is illustrated in Figure 4 and Figure 5.

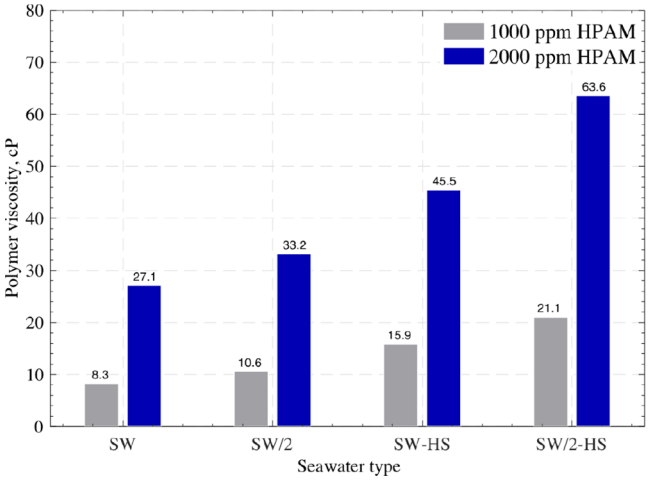

Figure 4. Rheology test: HPAM concentration effect at 25 °C.

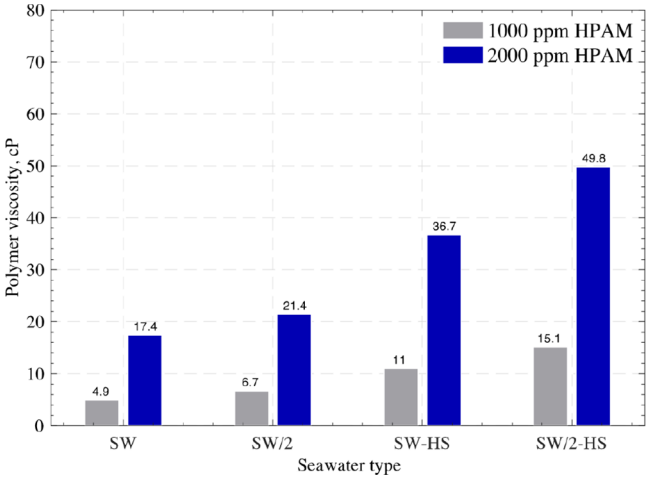

Figure 5. Rheology test: HPAM concentration effect at 60 °C.

Under the same conditions, the viscosity of 2000 ppm HPAM was twice to 3.5 times as large as that of 1000 ppm HPAM. In the low-shear rate region, the viscosity difference between the two concentrations was larger than that in the high-shear rate region. This is in line with the experimental results from the literature, in which an HPAM-based polymer solution was tested.[21] Under 60 °C, the smallest viscosity of polymer solution is 4.9 cP, which is sufficient to moblize the bypassed crude oil.

The effects of salinity and hardness of the base fluids (SW, SW/2, SW-HS, and SW/2-HS) and shear rate on polymer viscosity are illustrated in Figure 6.

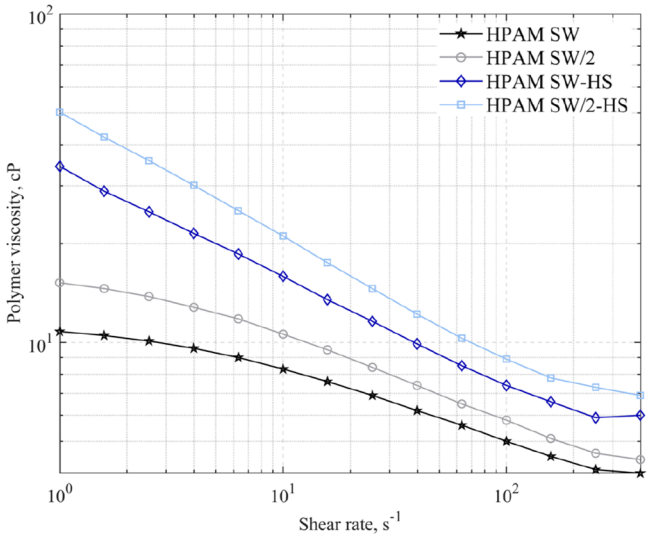

Figure 6. Rheology test: HPAM salinity and hardness effect, 1000 ppm.

In the bulk rheology test, all HPAM solutions exhibited shear-thinning behavior under shear rates from 1 to 400 s^{-1}. Early in the 1970s, the shear-thinning feature of HPAM has been reported.[22] When the shear rate increases, the polymer coils were forced apart by shear forces, leading to viscosity reduction.[23] The viscosity of polyacrylamide solutions in the shear-thinning region can be described using a power law model[24,25]

$$\eta = K\dot{\gamma}^{n-1} \tag{6}$$

where η represents the viscosity in Pa·s, K represents the consistency index in Pa·s, $\dot{\gamma}$ represents the shear rate in s^{-1}, and n represents the flow index. In Figure 6, the viscosity curves in the double-log scale show a linear trend versus shear rates, indicating that they satisfy the power law behavior. K and $\dot{\gamma}$ can be determined according to the slope of the viscosity−shear rate curve.

Under the same conditions, the viscosities of the polymer solutions, in descending order, were SW/2-HS > SW-HS > SW/2 > SW. When the salinity and hardness of the base fluid were higher, the viscosity of the polymer solution decreased. After hydrolysis, the acrylate moieties with anionic chargers were associated with cations, and the viscosity of the polymer solutions decreased towards the viscosity of the non-hydrolyzed polymer.[26] In addition, compared with salinity, hardness of base fluids had a more pronounced effect on lowering the polymer viscosity because divalent cations (Ca^{2+} and Mg^{2+}) could connect two acylate moieties together, leading to the direct shrinking of the hydraulic radius of polymer molecules in addition to decreasing the intramolecular repulsions.[26] Consequently, the viscosity loss is much more if there are

https://doi.org/10.1021/acsomega.3c01984
ACS Omega 2023, 8, 24426−24440

divalent cations in the base fluids, which has been reported in the literature.[27]

The effect of ions on the viscosity of the electrolyte was studied. To understand the viscosity of electrolyte solutions, Falkenhagen and Vernon[28] proposed an electrostatic model describing the distribution of ions in relation to electrolyte solutions and viscosity of dilute solutions of strong electrolytes. Kaminsky[29] reported the viscosity of aqueous solutions of strong electrolytes at different temperatures and concentrations to investigate how viscosity changes of aqueous solutions depend on interionic forces and particularly on ion−solvent interactions. Electrokinetics has been utilized to design matrix low-concentration acid stimulation and has been proven to be a useful approach for EOR or IOR application.[30,31] According to the Arrhenius ionic theory, the molecules of electrolytes in aqueous solution (seawater) spontaneously dissociate to form cations (Na^+, Ca^{2+}, and Mg^{2+}) and anions (Cl^-, SO_4^{2-}, and HCO_3^-). Wang et al.[32] have explained the behavior of polymer viscosity in different seawater formulations using the DLVO theory. It is reported that when the electrolyte (HPAM) is added to solutions, the dissociated cations from salt can compress the thickness of the electrical double layer (EDL) of HPAM, leading to the reduction in the charge of the HPAM molecule, which in turn results in a decrease in the interaction between the polymer chains and subsequent reduction in the viscosity of the polymer solution.[32] It is also mentioned that the divalent cations are more effective in shielding the negative charge on the HPAM molecule chain due to higher charge densities of divalent cations (Ca^{2+}, and Mg^{2+}) compared to ionic cations (Na^+).[32]

An interesting phenomenon is that, with divalent ions, the polymer viscosity reduction with an increasing shear rate was lower (Figure 6). At a low shear rate, the polymer molecule coils were compacted in the base fluid without divalent ions. When the shear forces increased owing to the high shear rate, the compacted polymer coils were forced apart, leading to a reduction in polymer viscosity. If there are divalent ions in the base fluid, even at low shear rates, the divalent cations will effectively shield the negative charge on the polymer molecule chain, thus shrinking the EDL and hydraulic radius of the polymer molecules and leading to a lower viscosity. The increasing shear forces due to the higher shear rate will further separate the coils and lower the viscosity, but the viscosity difference due to shear rate elevation will not be observed in the low-divalent-ion case. Electrochemical mechanisms, such as the EDL, play an important role in analyzing the interactions between injecting chemicals during EOR. Olayiwola and Dejam[33] developed a mathematical model to describe the surface tension/IFT for different systems of nanoparticles (NPs), surfactants, and electrolytes, in which the cohesive energy, EDL effect, and dipole−dipole interaction of NPs and electrolytes. Olayiwola and Dejam[34] also reviewed the interaction mechanisms of NPs with the low salinity water (LSW) and surfactant for EOR, including the EDL effect. The aggregation mechanism of NPs occurring when 3 wt % of NaCl is added to 0.5 wt % of silica NPs is also reviewed and attributed to screening charges and the EDL because of high salinity.[35]

To avoid chemical degradation, diluting the seawater or stripping out the divalent cations from seawater to reduce the salinity and hardness of the base fluids might help maintain polymer viscosity. The latter approach might be more efficient but requires more investment in surface facilities.

Under a constant shear rate of 10 s^{-1}, the effect of temperature on the polymer viscosity was studied at temperatures ranging from 25 to 60 °C, as illustrated in Figure 7.

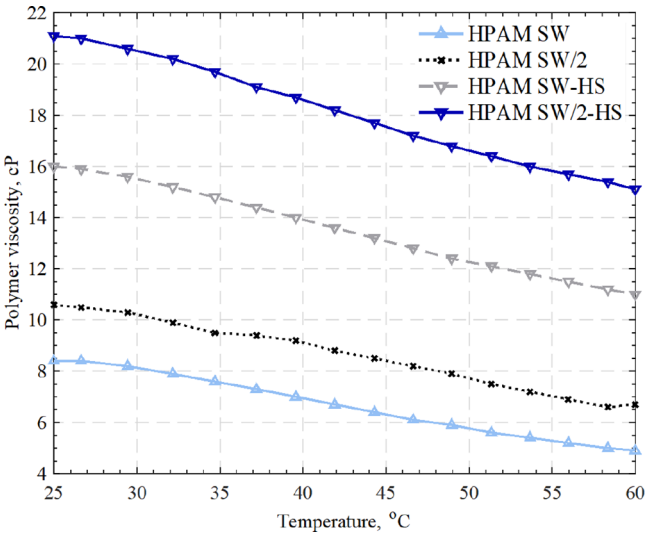

Figure 7. Rheology test: HPAM temperature effect, 1000 ppm.

Under the same conditions, the polymer viscosity, in descending order, was SW/2-HS > SW-HS > SW/2 > SW. Thermal degradation refers to the free radical breakdown of the acrylic backbone, leading to molecular weight reduction and viscosity loss, while chemical degradation refers to the hydrolysis of polymer functional groups.[26,36]

From the perspective of chemical degradation, hydrolysis of the amide moiety would cause anionic charges on the acylate moieties, which would increase the hydrodynamic radius and hence the polymer viscosity. The acrylate moieties with anionic charges are strongly associated with cations, and the solution viscosity decreases toward the viscosity of the non-hydrolyzed polymer.[21,23] From the perspective of thermal degradation, the free radical breakdown of the acrylic backbone also took place, exhibiting viscosity loss with elevated temperatures.[21] The intergaretd effect of chemical degradation and thermal degradation would lead to the viscosity drop, which has been reported in the literature.[7,20,22,24−26]

The effects of the shear rate, salinity, and hardness of the base fluids and temperature on the SAP viscosity were investigated. The viscosities of the four SAP solutions versus shear rate and temperature are illustrated in Figures 8 and 9, respectively.

Under the same conditions, the viscosities of the polymer solutions, in descending order, were SW/2-HS > SW-HS > SW/2 > SW. When the salinity and hardness of the base fluid were high, the viscosity of the polymer solution decreased. In addition, the hardness of the base fluids has a more pronounced effect on lowering polymer viscosity. SAP SW-HS and SAP SW/2-HS exhibited shear-thickening behavior under a shear rate from 1 to 10 s^{-1}. This might be due to the extension of polymer molecules in this shear-rate region, leading to shear-extended viscosity in addition to the initial viscosity. A physical interaction might exist that links a few polymer molecules together and causes an increase in viscosity. The presence of divalent cations (Ca^{2+} and Mg^{2+}) in the base fluid may also be related to the fact that SAP SW and SAP SW/2 did not exhibit shear-thickening features.

https://doi.org/10.1021/acsomega.3c01984
ACS Omega 2023, 8, 24426−24440

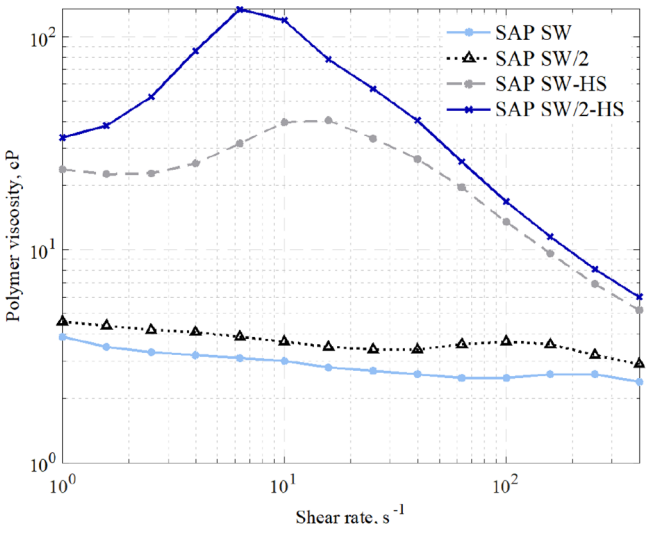

Figure 8. Viscosity of SAP solutions versus shear rate.

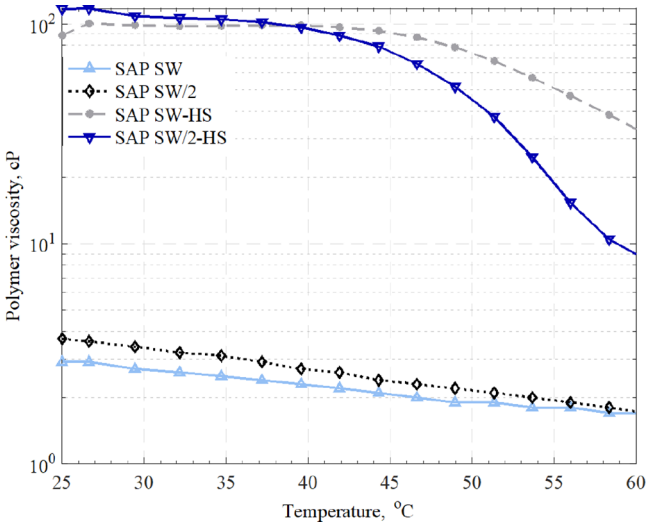

Figure 9. Viscosity of SAP solutions versus temperature.

At a fixed shear rate of 10 s^{-1}, the viscosity of the SAP solutions was measured at temperatures ranging from 25 to 60 °C. The viscosity of the polymer solutions decreased with increasing temperature. The integrated effect of chemical and thermal degradation leads to a drop in viscosity. Initially, under the same conditions, the polymer viscosity decreased in the following order: SW/2-HS > SW-HS > SW/2 > SW. When the temperature was increased above 40 °C, the viscosity of SAP SW/2-HS became lower than that of SAP SW-HS. The irregular viscosity loss patterns of SAP SW-HS and SW/2-HS might be attributed to the retarding effect of high salinity on thermal degradation.

In Table 9, the viscosities of the two polymers in typical shear rate regions (1−15.8 s^{-1}) are compared. From 1 to 10 s^{-1}, the SAP polymer exhibited shear-thickening features; thus, the viscosity increased significantly. Between 10 and 15.8 s^{-1}, the SAP polymer exhibited shear-thinning even though the shear-thickening SAP at a shear rate of 15.8 s^{-1} still had very high viscosities (40−78 cP). In comparison, although HPAM had a relatively higher upper bound of the initial viscosity, it exhibited shear-thinning features in the full shear-rate region. Consequently, HPAM had much lower viscosities at higher shear rates (8−21 cP at 10 s^{-1} and 8−18 cP at 15.8 s^{-1}). The SAP exhibited shear-thickening features in engineered seawater. However, for HPAM, engineering the formulations of seawater only increased their initial viscosity (at 1 s^{-1}) and lowered their shear-thinning rate (Figures 6 and 8).

Table 9. Comparison of Polymer Viscosities in the Typical Shear Rate Region (Data from Figures 6 and 8)

shear rate, s^{-1}	1	10	15.8
viscosity range of (shear-thickening) SAP, cP	24−34	40−119	40−78
viscosity range of HPAM	11−50	8−21	8−18

After the bulk rheology test, four HPAM solutions and four SAP solutions were shortlisted for the upcoming formation damage test and the oil displacement efficiency experiment. The concentration of the polymer solution was 1000 ppm. Eight experiments using these eight polymer solutions would be tested under the FB-1 condition, and eight polymer solutions would be tested under the FB-2 condition.

3.2. Formation Damage Induced by Polymer Injection. The results of the HPAM and SAP experiments are shown in Figures 10 and 11, respectively. In both figures, the

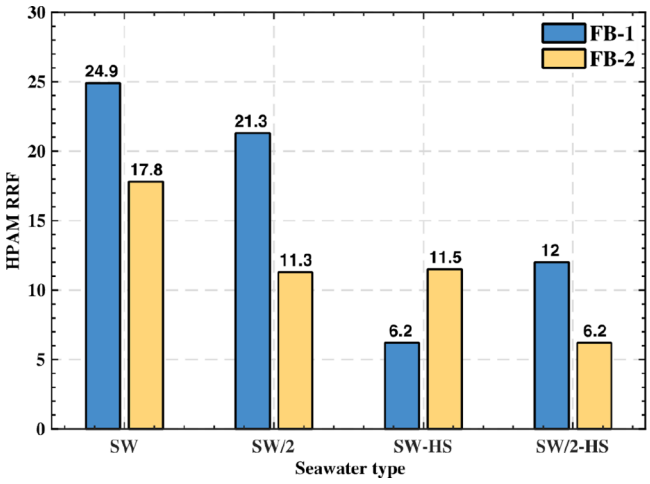

Figure 10. RRF values of HPAM solutions in porous media.

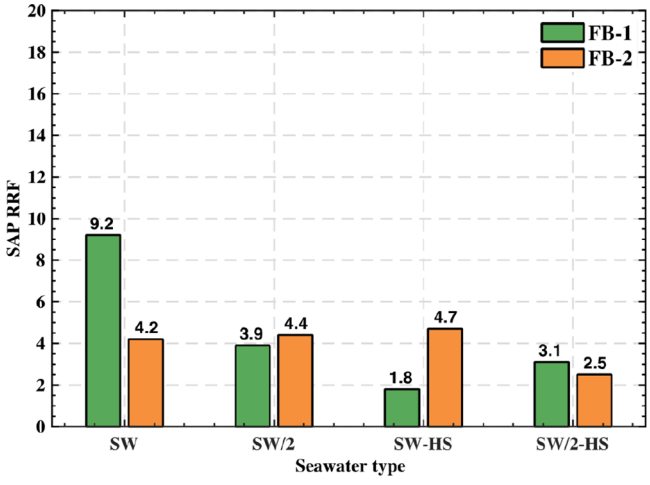

Figure 11. RRF values of SAP solutions in porous media.

https://doi.org/10.1021/acsomega.3c01984
ACS Omega 2023, 8, 24426−24440

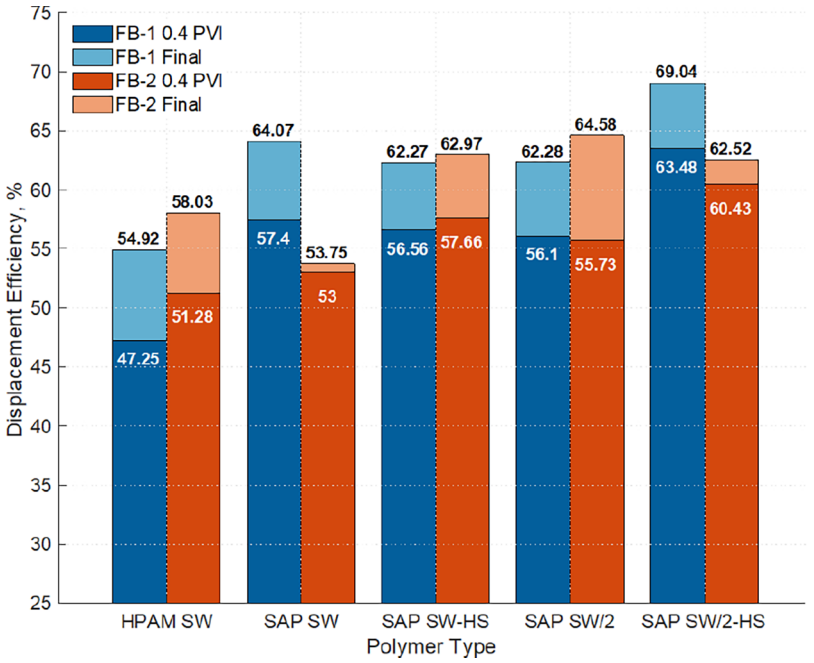

Figure 12. Oil displacement efficiency after polymer flooding.

RRF values are on the *Y* axis and different types of base fluids are on the *X* axis. In this study, eight core plugs were saturated in FB-1, while eight core plugs were saturated in FB-2. The RRF results were affected by the composition (salinity and hardness) of the formation brines. The factors affecting RRF, such as the formation brine type, polymer type, and composition of base fluids, were analyzed.

Based on the experimental results, the key findings are the following:

For HPAM and SAP solutions under both formation brine conditions, the RRF was lower when the salinity and hardness of the base fluid were lower, indicating that the formation damage effect was more serious when the base fluid had higher salinity and hardness. The underlying mechanisms are polymer precipitation and fluid−rock interactions. The impact of the ion composition on the polymer or electrolyte viscosity has been well explained.[32,37−40] The cations can shield the negative charge on the polymer molecule chain and shrink the hydraulic radius of the polymer molecules, leading to a lower viscosity. Divalent cations have a more effective shielding effect and can cause greater viscosity reduction. The polymers might precipitate during this process, and divalent cations can lead to more severe polymer precipitation.[37] The precipitation might become trapped in the pore space and lead to permeability impairment. This explains the phenomenon that with increasing salinity and hardness, not only the viscosity of the polymer solutions decreased but also the RRF increased (more formation damage). The other potential mechanism is the fluid−rock interaction. Bishop[41] investigated the formation damage of sandstone induced by injection of high-salinity brine through core-flooding experiments and found that high-salinity brine invasion caused flocculation of the pore lining clays and led to significant permeability impairment. The cations, especially divalent cations (HPAM SW-HS case), might interact with negatively charged sandstone and lead to permeability impairment. This might also cause a higher RRF when using polymer base fluids with high salinity and hardness. For the HPAM solutions, from the FB-1 condition to the FB-2 condition, the RRF has a decreasing trend, except for HPAM SW-HS. This might be attributed to the fact that the contact of FB-2 with residual polymers accelerated the breakdown of polymer molecules, leading to less formation damage. Another potential explanation is that the presence of FB-2 reduced the ion interaction between the polymer solution and porous media.

Under the same temperature and formation brine conditions, the RRF values of the SAP polymer solutions were much lower than those of the HPAM polymer solutions. The supporting evidence is that the lower molecular weight of SAP (0.5 million Daltons) compared with that of HPAM (15 million Daltons) might contribute to less mechanical entrapment of SAP molecules, leading to less formation damage.

Based on the current experimental data, the integrated benefits of better mobility control ability and less formation damage effect make SAP a better candidate for polymer coreflood experiments and potential EOR applications.

The polymer solutions for the oil displacement efficiency experiments were further shortlisted according to the results of the bulk rheology tests and formation damage tests. Under both formation brine conditions, four SAP solutions (SAP SW, SAP SW-HS, SAP SW/2, and SAP SW/2-HS) and one HPAM solution (HPAM SW) were used to investigate the polymer flooding effect on the oil displacement efficiency.

3.3. Oil Displacement Efficiency Study. The displacement efficiency results are summarized in Figure 12.

The *Y* axis of this figure is the oil displacement efficiency, including the displacement efficiency of 0.4 PV polymer injection and final displacement efficiency. The *X* axis illustrates the five polymer solutions used in the experiments; the blue color represents the FB-1 condition, and the orange color represents the FB-2 condition. Ten oil displacement efficiency experiments were conducted. Overall, the displacement efficiencies of the SAP solutions were higher than those of the HPAM solutions. The highest DE was 69.04% when SAP SW/2-HS was used under the FB-1 condition.

https://doi.org/10.1021/acsomega.3c01984
ACS Omega 2023, 8, 24426−24440

3.3.1. Case I: HPAM SW. Figures 13 and 14 illustrate the DE, water cut, and pressure drop vs the injected PV of the

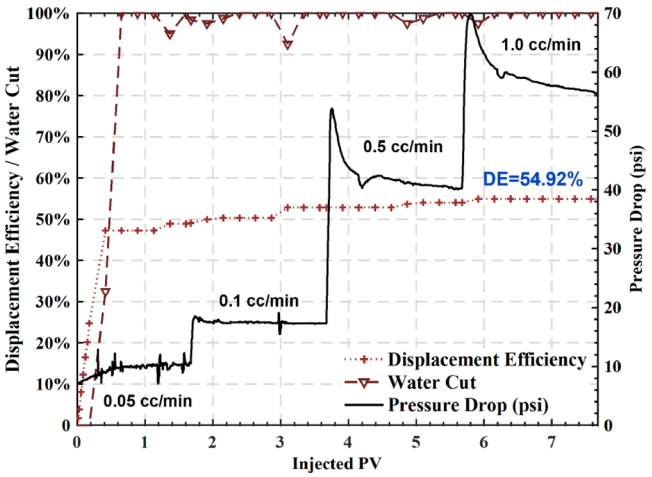

Figure 13. HPAM SW in FB-1: DE, WC, and pressure drop vs injected PV.

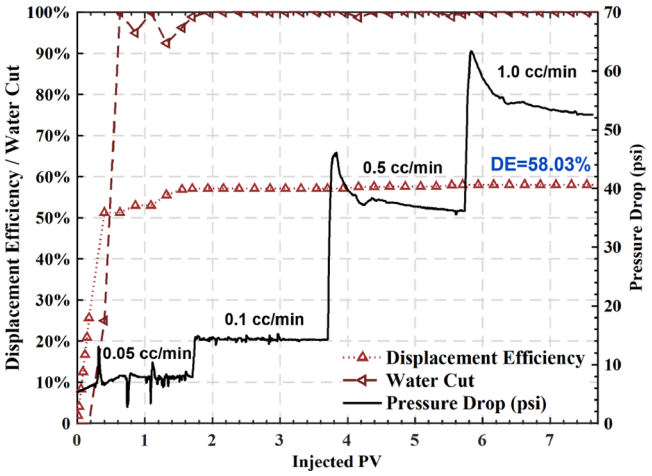

Figure 14. HPAM SW in FB-2: DE, WC, and pressure drop vs injected PV.

polymer solution. The first condition was FB-1, and the second was FB-2. First, around 1.6 PV of polymer was injected with the 1 ft/day flow rate followed by 2 PV of next injection rate. The DE for each experiment was then recorded.

According to Figure 12, the displacement efficiency after 0.4 PV of polymer injection and the final DE are lower than those of the other SAP experiments. This indicates the lower mobility control ability of HPAM, which may be related to its degradation in porous media and shear-thinning features. The shear-thinning feature of HPAM was observed in the bulk rheology test (Figure 6), and serious formation damage was reflected in the high RRF values calculated from the formation damage test (Figure 10).

3.3.2. Case II: SAP SW. Figures 15 and 16 illustrate the DE, water cut, and pressure drop vs injected PV of the SAP SW experiments in each formation brine condition.

Figure 12 illustrates that the displacement efficiency of SAP SW after 0.4 PV of polymer injection is higher than those of the HPAM experiments, especially under the FB-1 condition. This indicates that compared with HPAM prepared in seawater, the SAP prepared in seawater might have a higher

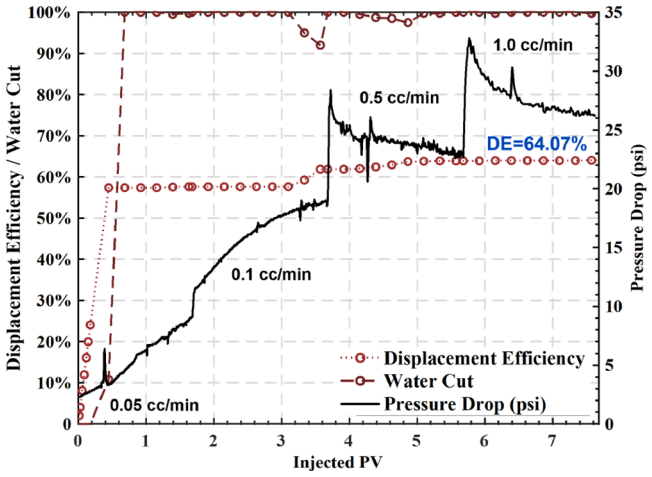

Figure 15. SAP SW in FB-1: DE, WC, and pressure drop vs injected PV.

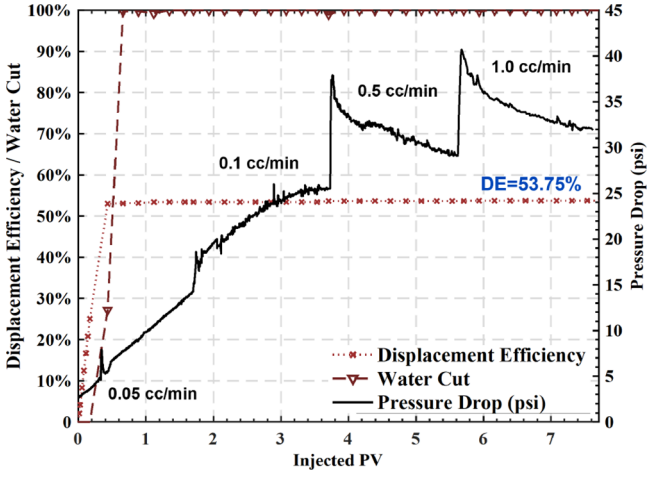

Figure 16. SAP SW in FB-2: DE, WC, and pressure drop vs injected PV.

EOR performance. Thus, it may be able to produce the oil more efficiently. In addition, less formation damage was reflected by the lower RRF values compared with the HPAM solutions under the same conditions (Figure 10).

3.3.3. Case III: SAP SW-HS. Figures 17 and 18 illustrate the DE, water cut, and pressure drop vs injected PV of the SAP SW-HS under each formation brine condition.

According to Figure 12, the final displacement efficiencies under both FB conditions were similarly high. Additionally, the displacement efficiencies of 0.4 PV polymer injection under both FB brines conditions are similarly high. This indicates the high EOR performance of SAP SW-HS and low formation damage. The displacement efficiencies were not significantly affected by the FB brines.

Regarding the RRF values under both formation brine conditions from the formation damage test (Figure 10), the RRF under the FB-1 condition was lower than that under the FB-2 condition. This indicates lower formation damage under the FB-1 condition, even when the EOR performance is similar.

3.3.4. Case IV: SAP SW/2. Figures 19 and 20 illustrate the DE, water cut, and pressure drop vs injected PV of the SAP SW/2 under each formation brine condition.

https://doi.org/10.1021/acsomega.3c01984
ACS Omega 2023, 8, 24426−24440

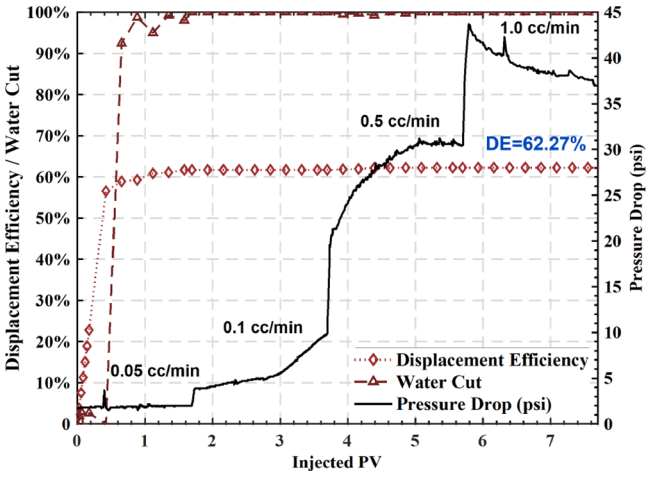

Figure 17. SAP SW-HS in FB-1: DE, WC, and pressure drop vs injected PV.

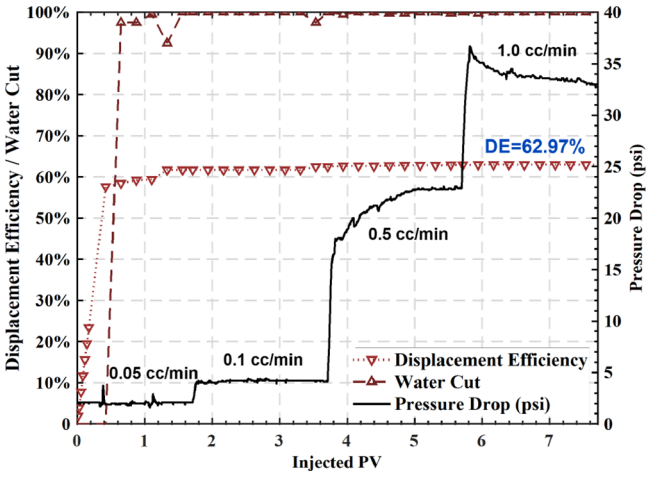

Figure 18. SAP SW-HS in FB-2: DE, WC, and pressure drop vs injected PV.

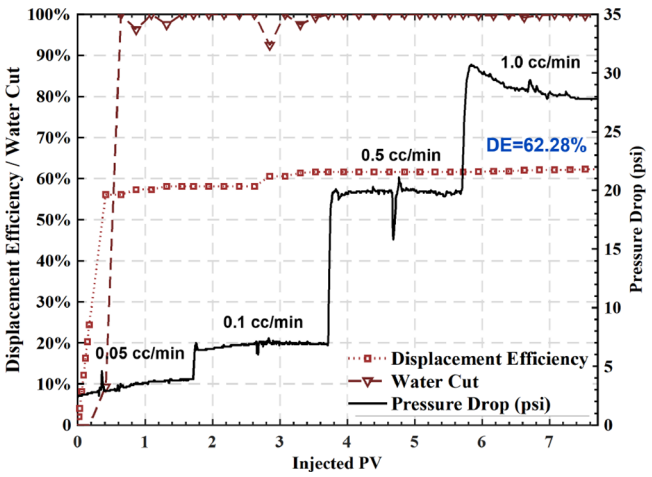

Figure 19. SAP SW/2 in FB-1: DE, WC, and pressure drop vs injected PV.

First, according to Figure 12, for this polymer solution, the displacement efficiency after 0.4 PV of polymer injection and the final DE are similar and in a high range under both formation brine conditions. This indicates that SAP SW/2 has high EOR performance and low formation damage (Figure 10). Second, when comparing the RRF values of this case with the RRF values of the SAP SW-HS case from the formation damage test, it was found that under the FB-1 condition, SAP SW-HS had a much lower RRF. This indicates that although the DE performance is similar, SAP SW/2 caused more formation damage than SAP SW-HS.

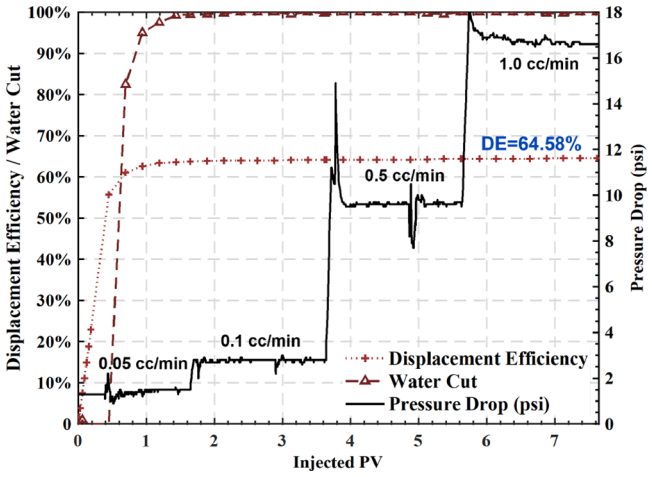

Figure 20. SAP SW/2 in FB-2: DE, WC, and pressure drop vs injected PV.

3.3.5. Case V: SAP SW/2-HS. The last case is the SAP SW/2-HS under each formation brine condition. Figures 21 and 22 illustrate the DE, water cut, and pressure drop vs injected PV of polymer solution. he first one was the FB-1 condition, and the second one was under the FB-2 condition.

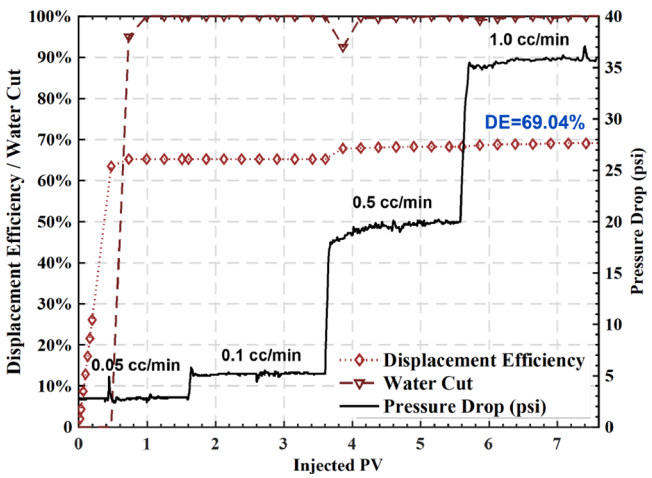

Figure 21. SAP SW/2-HS in FB-1: DE, WC, and pressure drop vs injected PV.

First, according to Figure 12, for this polymer solution, the displacement efficiency after 0.4 PV of polymer injection is the highest under both formation brine conditions. In addition, both final DEs were in a high range, and especially under the FB-1 condition, the final DE was the highest among all experiments. This indicates that SAP SW/2-HS has the highest EOR performance with low formation damage, which is in line with the shear-thickening behavior of SAP indicated by the bulk rheology test (Figure 8) and RRF of SAP (Figure 10). Second, comparing the performance with SAP SW, under both

https://doi.org/10.1021/acsomega.3c01984
ACS Omega 2023, 8, 24426−24440

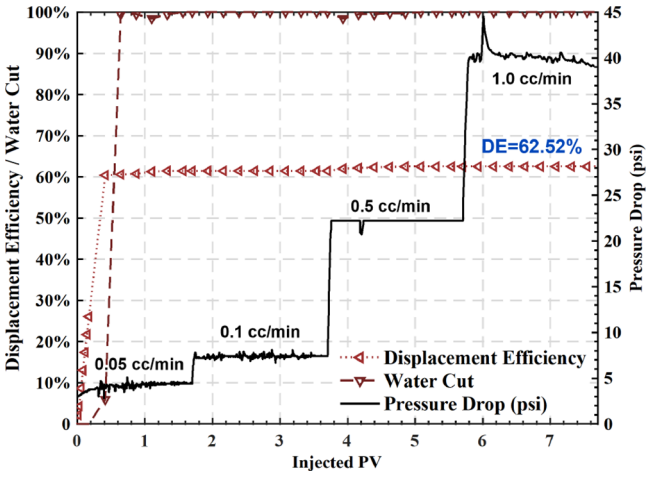

Figure 22. SAP SW/2-HS in FB-2: DE, WC, and pressure drop vs injected PV.

formation brine conditions, the displacement efficiencies of SAP SW/2-HS after 0.4 PV of polymer injection and final DE were much higher than those of SAP SW. In addition, the major displacement efficiency difference was from the period of 0.4 PV polymer injection, which was around 6−7%. The incremental oil DE from 0.4 PV to the end of polymer injection was similar under each formation brine condition. An indication is that the SW/2-HS contributed to higher performance of SAP mainly in the first 0.4 PV of polymer injection.

3.4. Discussion. Ten core-flood experiments were conducted to investigate the EOR performance of HPAM and SAP prepared in different engineered brine formulations under harsh reservoir conditions.

The improved oil recovery potential due to the shear thickening of SAP polymer solutions compared to the regular HPAM polymer was proven in this study. Under FB-1 (lower salinity and hardness) and FB-2 (higher salinity and hardness) conditions, SAP prepared in hardness-stripped brine (SW/2-HS, SW-HS) achieved the highest displacement efficiency. This can be attributed to the shear-thickening feature of SAP. Under both formation brine conditions, SAP SW/2-HS exhibited the highest EOR performance followed by SAP SW-HS (Figure 11). The better EOR performance when using hardness-stripped brine to prepare polymer solutions validated the results that divalent cations played an important role in lowering the polymer viscosity and causing more serious formation damage.

4. SUMMARY AND CONCLUSIONS

This study comprehensively investigated the EOR performance of normal HPAM and shear-thickening polymer SAP prepared in different formulations of engineered brines under harsh conditions (high temperature and high salinity) using 10 core-flooding experiments. It was confirmed that the shielding effect of cations on the negative charge of polymer molecules is responsible for polymer viscosity reduction, and divalent ions have a more pronounced impact. The potential precipitation of polymers in porous media caused by the shielding effect of cations, especially divalent cations, can also cause plugging and lead to additional formation damage. SAP exhibited shear-thickening behavior in bulk rheology tests compared to the power-law behavior of HPAM, which resulted in better recovery efficiency in the core-flooding experiments. The conclusions of this study are as follows:

(1) HPAM shows shear-thinning behavior in the shear rate region from 1 to 400 s^{-1} and exhibits a power-law behavior. In contrast, SAP prepared in hardness-stripped brine exhibits shear-thickening behavior in the low shear rate region (from 1 s^{-1} to approximately 10 s^{-1}). Short-term thermal degradation occurred in both the HPAM and SAP.

(2) Cations in engineered brine have a shielding effect on the negative charge of the polymer molecular chain and can shrink the EDL of the polymer, resulting in a reduction in polymer viscosity. Divalent ions have a more pronounced impact on reducing polymer viscosity because of the higher density of charges.

(3) In the presence of divalent cations, the reduction in polymer viscosity with the increasing shear rate was lower. Even under a low shear rate, the divalent cations effectively shrink the EDL and thus cause lower viscosity, which makes the potential of further lowering the polymer viscosity (by increasing shear rates) much smaller.

(4) The shielding effect of cations, especially divalent cations, can cause polymer precipitation, resulting in plugging of the pore space and thus permeability impairment. Another potential mechanism of the higher RRF due to high salinity and hardness might be that the interaction between cations (especially divalent cations) and negatively charged sandstone can cause permeability impairment.

(5) The formation damage caused by SAP is lower than that caused by HPAM, which can be attributed to the lower molecular weight of SAP compared to HPAM. The presence of more cations in FB-2 may reduce the ion interaction between the polymer solution and porous media, leading to a relatively lower RRF.

(6) In core-flooding experiments, the SAP prepared in hardness-stripped brine (SW/2-HS and SW-HS) achieved the highest displacement efficiency. This demonstrates the effectiveness of the shear thickening feature on the EOR. By combining these conclusions, the role of divalent cations in lowering polymer viscosity and causing more serious formation damage has been demonstrated. The ionic composition of the base fluid should be engineered to prepare a polymer solution for EOR implementation under specific reservoir conditions.

Based on the current experimental conditions, the SAP polymer demonstrated a good potential for EOR performance.

AUTHOR INFORMATION

Corresponding Author

Md Motiur Rahman − *Khalifa University of Science and Technology, Abu Dhabi 127788, United Arab Emirates;* orcid.org/0000-0002-4453-9230; Email: md.rahman@ku.ac.ae

Authors

Chuangchuang Qi − *Khalifa University of Science and Technology, Abu Dhabi 127788, United Arab Emirates;* orcid.org/0000-0002-6174-0972

Mohamed Haroun − *Khalifa University of Science and Technology, Abu Dhabi 127788, United Arab Emirates*

https://doi.org/10.1021/acsomega.3c01984
ACS Omega 2023, 8, 24426−24440

Abhijith Suboyin − *Khalifa University of Science and Technology, Abu Dhabi 127788, United Arab Emirates*
Jassim Abubacker Ponnambathayil − *Khalifa University of Science and Technology, Abu Dhabi 127788, United Arab Emirates;* orcid.org/0000-0002-8368-3139
Bisweswar Ghosh − *Khalifa University of Science and Technology, Abu Dhabi 127788, United Arab Emirates;* orcid.org/0000-0002-0413-6832

Complete contact information is available at: https://pubs.acs.org/10.1021/acsomega.3c01984

Notes

The authors declare no competing financial interest.

■ ACKNOWLEDGMENTS

The authors would like to sincerely thank Khalifa University of Science and Technology for the support to conduct and publish this work.

■ NOMENCLATURE

γ_w=shear rate [s^{-1}]
q=flow rate [cm^3/s]
A=cross-sectional area [cm^2]
K=absolute permeability [cm^2]
λ_w=water phase mobility
$\lambda_{w,\ initial}$=brine mobility before polymer injection
$\lambda_{w,\ after\ polymer}$=brine mobility after polymer injection
Δp=pressure drop during injection of brine [atm]
$\Delta p_{(brine\ before\ polymer)}$=pressure drop measured during brine injection prior polymer flooding [atm]
$\Delta p_{(brine\ after\ polymer)}$=pressure drop measured during brine injection after polymer flooding [atm]
k_o=oil permeability [D]
μ=dynamic viscosity of crude oil [cP]
L=length of core plug [cm]
A=cross-sectional area of the core plug [cm^2]
DE=oil displacement efficiency
V_{ot}=cumulative oil production [cm^3]
S_{wir}=irreducible water saturation
V_p=pore volume of core plug [cm^3]
W_c=water cut
V_o=oil production in specific duration [cm^3]
V_w=water production in specific duration [cm^3]
η=viscosity of fluid [Pa.s]
K=consistency index [Pa·s]
$\dot{\gamma}$=shear rate [s^{-1}]

■ REFERENCES

(1) Gbadamosi, A. O.; Junin, R.; Manan, M. A.; Yekeen, N.; Augustine, A. Hybrid Suspension of Polymer and Nanoparticles for Enhanced Oil Recovery. *Polym. Bull.* **2019**, *76*, 6193−6230.
(2) Lake, L. W.; Johns, R.; Rossen, B.; Pope, G. A. *Fundamentals of Enhanced Oil Recovery*; Society of Petroleum Engineers: Richardson, TX, 2014; Vol. *1*, DOI: 10.2118/9781613993286.
(3) Buchgraber, M.; Clemens, T.; Castanier, L. M.; Kovscek, A. R. The Displacement of Viscous Oil by Associative Polymer Solutions. In *SPE Annual Technical Conference and Exhibition*; OnePetro, 2009, DOI: 10.2118/122400-MS.
(4) Sorbie, K. S. *Polymer-Improved Oil Recovery*; 1991, DOI: 10.1007/978-94-011-3044-8.
(5) Dowd, W. T. *Secondary and Tertiary Oil Recovery Processes*; The Interstate Oil Compact Commission: Oklahoma City, 1974, 100.
(6) Haroun, M.; Rahman, M. M.; Li, Y.; Jiang, C.; Ghedan, S.; De Bakker, J.; Wu, Y. Maximizing Oil Recovery Through Hybrid Smartwater Surface Active Polymer: A Novel Environomic EOR Technology. In *SPE Gas & Oil Technology Showcase and Conference*; OnePetro, 2019. DOI: 10.2118/198557-MS.
(7) Alfazazi, U.; AlAmeri, W.; Hashmet, M. R. Experimental Investigation of Polymer Flooding with Low-Salinity Preconditioning of High Temperature−High-Salinity Carbonate Reservoir. *J. Pet. Explor. Prod. Technol.* **2019**, *9*, 1517−1530.
(8) Algharaib, M.; Alajmi, A.; Gharbi, R. Improving Polymer Flood Performance in High Salinity Reservoirs. *J. Pet. Sci. Eng.* **2014**, *115*, 17−23.
(9) Almansour, A. O.; AlQuraishi, A. A.; AlHussinan, S. N.; AlYami, H. Q. Efficiency of Enhanced Oil Recovery Using Polymer-Augmented Low Salinity Flooding. *J. Pet. Explor. Prod. Technol.* **2017**, *7*, 1149−1158.
(10) Hashmet, M. R.; Qaiser, Y.; Mathew, E. S.; AlAmeri, W.; AlSumaiti, A. M. Injection of Polymer for Improved Sweep Efficiency in High Temperature High Salinity Carbonate Reservoirs: Linear X-Ray Aided Flood Front Monitoring. In *SPE Kingdom of Saudi Arabia Annual Technical Symposium and Exhibition*; Day 4 Thu, April 27, 2017; OnePetro: Dammam, Saudi Arabia, 2017; p D043S040R003. DOI: 10.2118/188125-MS.
(11) Piñerez Torrijos, I. D.; Puntervold, T.; Strand, S.; Austad, T.; Bleivik, T. H.; Abdullah, H. I. An Experimental Study of the Low Salinity Smart Water - Polymer Hybrid EOR Effect in Sandstone Material. *J. Pet. Sci. Eng.* **2018**, *164*, 219−229.
(12) Meng, W.; Haroun, M. R.; Sarma, H. K.; Adeoye, J. T.; Aras, P.; Punjabi, S.; Rahman, M. M.; Al Kobaisi, M. A Novel Approach of Using Phosphate-Spiked Smart Brines to Alter Wettability in Mixed Oil-Wet Carbonate Reservoirs. In *Abu Dhabi International Petroleum Exhibition and Conference*; OnePetro, 2015, DOI: 10.2118/177551-MS.
(13) AlSofi, A. M. *The Simulation and Design of Polymer Flooding*; 2011. DOI: 10.25560/7031.
(14) Delshad, M.; Kim, D. H.; Magbagbeola, O. A.; Huh, C.; Pope, G. A.; Tarahhom, F. Mechanistic Interpretation and Utilization of Viscoelastic Behavior of Polymer Solutions for Improved Polymer-Flood Efficiency. In *SPE Symposium on Improved Oil Recovery*; OnePetro: Tulsa, Oklahoma, USA, 2008; p SPE-113620-MS. DOI: 10.2118/113620-MS.
(15) Choi, S. K.; Sharma, M. M.; Bryant, S. L.; Huh, C. PH Sensitive Polymers for Novel Conformance Control and Polymerflood Applications. In *SPE International Symposium on Oilfield Chemistry*; OnePetro, 2009. DOI: 10.2118/121686-MS.
(16) Koh, H.; Lee, V. B.; Pope, G. A. Experimental Investigation of the Effect of Polymers on Residual Oil Saturation. *SPE J.* **2018**, *23*, 1−17.
(17) Vermolen, E. C. M.; Pingo Almada, M.; Wassing, B. M.; Ligthelm, D. J.; Masalmeh, S. K. Low-Salinity Polymer Flooding: Improving Polymer Flooding Technical Feasibility and Economics by Using Low-Salinity Make-up Brine. In *International petroleum technology conference*; IPTC, 2014, DOI: 10.2523/IPTC-17342-MS.
(18) Qi, C.; Rabbani, A. I.; Suboyin, A.; Ponnambathayil, J. A.; Rahman, M. M.; Haroun, M.; Ma, Q.; Gibrata, M. A.; Rouis, L.; Djanuar, Y. Evaluation and Understanding the Potential of Enhanced Oil Recovery for a Candidate Offshore Sandstone Field. *In International Conference on Offshore Mechanics and Arctic Engineering*; American Society of Mechanical Engineers, 2022. DOI: 10.1115/OMAE2022-79074.
(19) Rabbani, A. I.; Al-Hajri, S.; Hussain, K. S.; Blackbourn, G.; Qi, C.; Suboyin, A.; Ponnambathayil, J. A.; Rahman, M. M.; Haroun, M.; Gibrata, M. A.; Rouis, L.; Djanuar, Y. Reservoir Characterization of the Pliocene Red Series, Lam Field and Surrounding Areas, Offshore Western Turkmenistan. *J. Pet. Geol.* **2023**, *46*, 77−102.
(20) American Petroleum Institute. Production Department *Recommended Practices for Evaluation of Polymers Used in Enhanced Oil Recovery Operations*; American Petroleum Institute, 1990; Vol. *63*.
(21) Alfazazi, U.; AlAmeri, W.; Hashmet, M. R. Screening of New HPAM Base Polymers for Applications in High Temperature and High Salinity Carbonate Reservoirs. In *Abu Dhabi International*

Petroleum Exhibition & Conference; OnePetro 2018, DOI: 10.2118/192805-MS.
(22) Mungan, N. Shear Viscosities of Ionic Polyacrylamide Solutions. *Soc. Pet. Eng. J.* **1972**, *12*, 469−473.
(23) Skauge, T.; Skauge, A.; Salmo, I. C.; Ormehaug, P. A.; Al-Azri, N.; Wassing, L. M.; Glasbergen, G.; Van Wunnik, J. N.; Masalmeh, S. K. Radial and Linear Polymer Flow - Influence on Injectivity. In *SPE Improved Oil Recovery Conference*; OnePetro, 2016. DOI: 10.2118/179694-MS.
(24) Transport Phenomena, R. B. Bird, W. E. Stewart, and E. N. Lightfoot, John Wiley and Sons, Inc., New York (1960). 780 Pages. $11.50. *AIChE Journal* **1961**, *7* (), 5J−6J, DOI: 10.1002/aic.690070245.
(25) Bonnier, J.; Rivas, C.; Gathier, F.; Quillien, B.; Thomas, A. Inline Viscosity Monitoring of Polymer Solutions Injected in Chemical Enhanced Oil Recovery Processes. In *SPE enhanced oil recovery conference*; OnePetro, 2013, DOI: 10.2118/165249-MS.
(26) Levitt, D.; Pope, G. A. Selection and Screening of Polymers for Enhanced-Oil Recovery. In *SPE symposium on improved oil recovery*; OnePetro, 2008, DOI: 10.2118/113845-MS.
(27) Jouenne, S. Polymer Flooding in High Temperature, High Salinity Conditions: Selection of Polymer Type and Polymer Chemistry, Thermal Stability. *Journal of Petroleum Science and Engineering* **2020**, *195*, No. 107545.
(28) Falkenhagen, H.; Vernon, E. L. LXII. The Viscosity of Strong Electrolyte Solutions According to Electrostatic Theory. *London, Edinburgh, Dublin Philos. Mag. J. Sci.* **1932**, *14*, 537−565.
(29) Kaminsky, M. Ion-Solvent Interaction and the Viscosity of Strong-Electrolyte Solutions. *Discuss. Faraday Soc.* **1957**, *24*, 171−179.
(30) Ansari, A.; Haroun, M.; Rahman, M. M.; Chilingar, G. V. Electrokinetic Driven Low-Concentration Acid Improved Oil Recovery in Abu Dhabi Tight Carbonate Reservoirs. *Electrochim. Acta* **2015**, *181*, 255−270.
(31) Ansari, A. A.; Haroun, M.; Rahman, M. M.; Chilingar, G. V. Increasing Depth of Penetration by Electrokinetic Driven Low-Concentration Acid IOR in Abu Dhabi Tight Carbonate Reservoirs. In *Abu Dhabi International Petroleum Exhibition and Conference*; OnePetro, 2014.
(32) Wang, Y.; He, Z.; Chen, W.; Liu, Y.; Ding, M.; Yang, Z.; Qian, C. Stability and Rheological Properties of HPAM/Nanosilica Suspensions: Impact of Salinity. *Colloids Surf., A* **2020**, *587*, No. 124320.
(33) Olayiwola, S. O.; Dejam, M. Interfacial Energy for Solutions of Nanoparticles, Surfactants, and Electrolytes. *AIChE J.* **2020**, *66*, No. e16891.
(34) Olayiwola, S. O.; Dejam, M. The Impact of Monovalent and Divalent Ions on the Viscosity of a Solution with Silica Nanoparticles. In *APS Division of Fluid Dynamics Meeting Abstracts*; APS Division of Fluid Dynamics, 2019, *A28*.004.
(35) Olayiwola, S. O.; Dejam, M. A Comprehensive Review on Interaction of Nanoparticles with Low Salinity Water and Surfactant for Enhanced Oil Recovery in Sandstone and Carbonate Reservoirs. *Fuel* **2019**, *241*, 1045−1057.
(36) Muller, G. Thermal Stability of High-Molecular-Weight Polyacrylamide Aqueous Solutions. *Polym. Bull.* **1981**, *5*, 31−37.
(37) Rostami, A.; Kalantari-Meybodi, M.; Karimi, M.; Tatar, A.; Mohammadi, A. H. Efficient Estimation of Hydrolyzed Polyacrylamide (HPAM) Solution Viscosity for Enhanced Oil Recovery Process by Polymer Flooding. *Oil Gas Sci. Technol.* **2018**, *73*, 22.
(38) Shakeel, M.; Pourafshary, P.; Hashmet, M. R. Investigation of Brine PH Effect on the Rheological and Viscoelastic Properties of HPAM Polymer for an Optimized Enhanced Oil Recovery Design. *ACS Omega* **2022**, *7*, 14961−14971.
(39) Olayiwola, S. O.; Dejam, M. Comprehensive Experimental Study on the Effect of Silica Nanoparticles on the Oil Recovery during Alternating Injection with Low Salinity Water and Surfactant into Carbonate Reservoirs. *J. Mol. Liq.* **2021**, *325*, No. 115178.
(40) Olayiwola, S. O.; Dejam, M. Experimental Study on the Viscosity Behavior of Silica Nanofluids with Different Ions of Electrolytes. *Ind. Eng. Chem. Res.* **2020**, *59*, 3575−3583.
(41) Bishop, S. R. The Experimental Investigation of Formation Damage Due to the Induced Flocculation of Clays Within a Sandstone Pore Structure by a High Salinity Brine. In *SPE European formation damage conference*; OnePetro, 1997, DOI: 10.2118/38156-MS.

https://doi.org/10.1021/acsomega.3c01984
ACS Omega 2023, 8, 24426−24440